CEBAF-PR 96-003
January 31, 1996

ATOMIC ELECTRON MOTION FOR MÖLLER POLARIMETRY IN A DOUBLE-ARM MODE

Andrei Afanasev
CEBAF, 12000 Jefferson Ave., Newport News, VA 23606, USA
and
NuHEP Center, Department of Physics, Hampton University, Hampton, VA 23668, USA
Alexander Glamazdin
CEBAF, 12000 Jefferson Ave., Newport News, VA 23606, USA

CONTINUOUS ELECTRON BEAM ACCELERATOR FACILITY

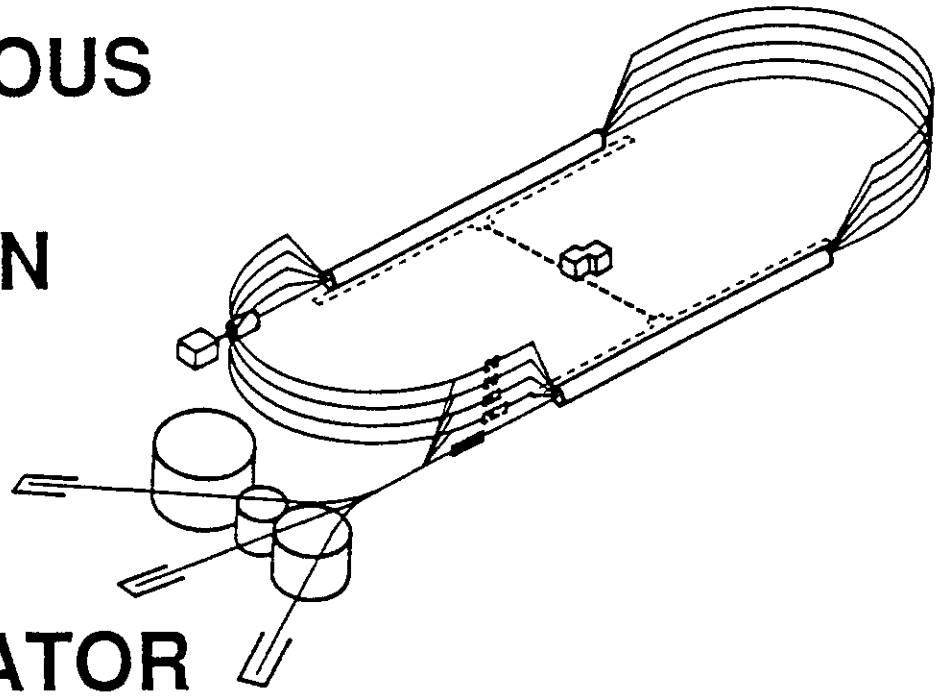

SURA *Southeastern Universities Research Association*

CEBAF
The Continuous Electron Beam Accelerator Facility
Newport News, Virginia

ATOMIC ELECTRON MOTION FOR MÖLLER POLARIMETRY IN A DOUBLE–ARM MODE

Andrei Afanasev*

CEBAF, 12000 Jefferson Ave., Newport News, VA 23606, USA

and

NuHEP Center, Department of Physics, Hampton University, Hampton, VA 23668, USA

Alexander Glamazdin†

CEBAF, 12000 Jefferson Ave., Newport News, VA 23606, USA

January 31, 1996

Abstract

We analyse an effect of electron Fermi motion at atomic shells on the accuracy of electron beam polarization measurements with a Möller polarimeter operating in a double–arm mode. It is demonstrated that the effect can result in either *increase* or *decrease* of the measured polarization depending on the detector positions. The effect is simulated for the Möller polarimeter to be installed at CEBAF Hall A.

To be submitted to Nuclear Instruments and Methods

*On leave from Kharkov Institute of Physics and Technology, Kharkov 310108, Ukraine

†Permanent address: Kharkov Institute of Physics and Technology, Kharkov 310108, Ukraine

1 Introduction

Möller polarimeters are widely used for electron beam polarization measurements in a GeV energy range. High quality of polarization experiments anticipated at new–generation CW multi–GeV electron accelerators such as CEBAF requires precise measurements of electron beam parameters. One of these parameters is the electron beam polarization. It can be measured by a Möller polarimeter.

There is a number of systematic corrections which should be accounted for when obtaining electron beam polarization from the asymmetry measured with a Möller polarimeter. They may be related to the knowledge of foil magnetization, accidentals, backgrounds, etc. An important systematic correction is due to electron Fermi–motion at atomic shells [2]. This correction is in principle different from the others listed above because it enters on the level of elementery ee-cross section. By analogy with radiative corrections, this correction may be called *internal* as opposed to external corrections. Therefore, the effect is present in any design of the Möller polarimeter, operating in either single–arm or coincidence modes.

Before the paper [2] was published, the effect of Fermi–motion at atomic shells was belived to negligible. However, the discrepancy between polarization values measured with Möller and Compton polarimeters at SLC/SLD demonstrated that this correction may be large, it was estimated to be 14% in this particular case [3].

In this paper, we report on some results obtained while developing a Möller polarimeter for Hall A at CEBAF. The paper is organized as follows. Section 2 describes the formalism for polarized ee-scattering and the effect of a target electron motion on the spin asymmetry. Section 3 lists basic results, and the conclusions are presented in Section 4.

2 Formalism

Möller polarimetry is based on scattering of polarized electron beam on a polarized electron target. The polarization dependent cross-section for the electron-electron scattering is given by [1]

$$\frac{d\sigma^{Möll}}{d\Omega^*} = \frac{d\sigma_0^{Möll}}{d\Omega^*}(1 + \sum_{i,j} P_i^b A_{ij} P_j^t), \tag{1}$$

$$(i, j = x, y, z),$$

where P_i^b (P_j^t) are components of the beam (target) polarization, A_{ij} are the asymmetry parameters, and $d\sigma_0^{Möll}/d\Omega^*$ is the cross–section for the unpolarized particles. Here we use the coordinate system with z–axis the electron beam direction and x–(y-) axis coplanar (normal) to the reaction plane.

Using one–photon exchange and the ultrarelativistic limit for the unpolarized cross–section and the nine asymmetry parameters one has

$$\frac{d\sigma_0^{Möll}}{d\Omega^*} = \frac{\alpha^2}{4m^2}\gamma^{-2}\frac{(4 - \sin^2\Theta^*)^2}{\sin^4\Theta^*}, \tag{2}$$

$$A_{zz} = -\frac{(7 + \cos^2\Theta^*)\sin^2\Theta^*}{(3 + \cos^2\Theta^*)^2}, \tag{3}$$

$$-A_{xx} = A_{yy} = \frac{\sin^4\Theta^*}{(3+\cos^2\Theta^*)^2}, \tag{4}$$

$$A_{zx} = A_{xz} = -\frac{2\sin^3\Theta^*\cos\Theta^*}{\gamma(3+\cos^2\Theta^*)^2}, \tag{5}$$

$$A_{xy} = A_{yx} = A_{zy} = A_{yz} = 0, \tag{6}$$

$$\gamma = \sqrt{\frac{(E_0+m)}{2m}},$$

where α is the fine–structure constant, Θ^* is the c.m.s. scattering angle, m is the electron mass, and E_0 is the energy of the incident electron in the laboratory system.

It is seen that at $\Theta^* = 90^0$ the asymmetry parameters A_{xx}, A_{yy} and A_{zz} are maximal

$$A_{zz} = -\frac{7}{9}, \quad A_{xx} = -\frac{1}{9}, \quad A_{yy} = \frac{1}{9}, \tag{7}$$

and the asymmetries A_{xz} and A_{zx} are small within the whole angular acceptance and vanish at 90^0.

In experiment, the polarized electron beam is incident on a magnetized ferromagnetic foil. The observed symmetry of Möller scattering from atomic electrons,

$$A = \frac{N_{\uparrow\uparrow} - N_{\uparrow\downarrow}}{N_{\uparrow\uparrow} + N_{\uparrow\downarrow}}, \tag{8}$$

gives the desirable polarization of the electron beam provided the target polarization is known.

Let us consider Möller scattering on a moving target electron from a particular atomic shell n. In the laboratory frame, cosine of the scattering angle is given by

$$\cos\Theta = \cos\Theta_0 + (\Delta\cos\Theta)_F, \tag{9}$$

where Θ (Θ_0) is a lab. scattering with (without) target electron motion, and the $(\Delta\cos\Theta)_F$ is a correction due to Fermi–motion of the target (denoted by P_F), and neglecting higher–order terms in expansion over E_0^{-1}, we obtain

$$(\Delta\cos\Theta)_F = \cos\Theta_{12}\frac{P_F^n}{m}(1-\cos\Theta_0), \tag{10}$$

where Θ_{12} is an angle between the momenta of the beam and the target electron. At $\Theta^* = 90^0$, Eq.(10) becomes

$$(\Delta\cos\Theta)_F = \cos\Theta_{12}\frac{P_F^n}{E_0}, \tag{11}$$

this result was reported earlier [4]. Eq.(11) can also be rewritten in the form

$$\Theta = \Theta_0\sqrt{1-\frac{P_F^n}{m}\cos\Theta_{12}}, \tag{12}$$

In the leading order of P_F/m expansion, it reproduces the original L. Levchuk's result (Eqs. 9-10 of Ref.[2]). However, for the case of large acceptances it is more consistent to use a general result Eqs. (9)-(10) herein, because angles far from $\Theta^* = 90^0$ are involved. Let us summarize the obtained results. Atomic electron motion does not affect the values of cross section and scattered electrons energies but it changes the angle of Möller scattering. A dominant effect comes from target electron motion parallel (antiparallel) to the direction of the incident beam; an effect from transverse target motion is supressed by an extra factor of $\sqrt{2m/E_0}$. Using the changed Möller kinematics described by Eqs.(9)–(10), one should take a sum over all atomic shells and integrate over Θ_{12} and P_F using a proper atomic wave function. To estimate the effect, we assume what $P_F^n = \sqrt{2m\varepsilon_B^n}$, ε_B^n being an electron binding energy at the atomic shell n.

Electrons in the atom of iron have the binding energies [5] listed in Table 1.

Table 1. Electron binding energies for ^{26}Fe (atomic moment=$2.22\mu_B$)

Shell	$K(1s)$	$L_I(2s)$	$L_{II}(2p_{1/2})$	$L_{III}(2p_{3/2})$	$M_I(3s)$	$M_{II,III}(3p)$	$M_{IV,V}(3d) + N_I(4s)$
ε_B^n, eV	7112	846.1	721.1	708.1	92.9	54.0	3.6±0.9
Number of electrons	2	2	3	3	2	6	$6(3d) + 2(4s)$

Thus, scattering from K- and L-shells smears the Möller scattering angle by $\Delta\Theta/\Theta \simeq \pm 10\%$ and $\pm 3\%$ respectively, around $\Theta^* = 90^0$. Only the electrons on the incomplete M-shell are polarized. (Iron needs 4 more electrons on $3d$-shell to complete it. Overlapping $3d$ and $4s$ levels in metal yield the observable hyromagnetic ratio of $2.22\mu_B$). The Möller asymmetry for electron-atom scattering may be presented as

$$A = \frac{\Sigma(\sigma_n(\uparrow\uparrow) - \sigma_n(\uparrow\downarrow))}{\Sigma(\sigma_n(\uparrow\uparrow) + \sigma_n(\uparrow\downarrow))}, \tag{13}$$

where the sum is taken over all n atomic shells, and $\sigma_n(\uparrow\uparrow)$ or $\sigma_n(\uparrow\downarrow)$ correspond to the Möller cross section with spins parallel or antiparallel, respectively. Only polarized (loosely bound) electrons from the M–shell contribute to the numerator in Eq.(13) r.h.s., whereas all electrons including strongly bound K–, L–shell ones, contribute to the denominator of Eq.(13) r.h.s. Therefore, kinematic smearing due to Fermi–motion affects the denominator, rather than the numerator for the asymmetry expression Eq.(13).

For a standard geometry of Möller polarimeters,when the detector(s) is(are) centred around $\Theta_{cm} = 90^0$, it may result in missing electrons scattered from K–, L–shells yielding a higher theoretical estimate for the asymmetry A. It was the basic conclusion of [2] confirmed later in SLAC/SLC measurements [3]. However, in contrast to original predictions [2], this effect does not exceed 2% for single–arm Möller measurements at MIT [6]. For the double–arm Möller polarimeter at MIT [7] a preliminary estimate done by one of us [4] predicts the correction to the Möller asymmetry to be around 12% , but this estimate may change if the magnetic field of the polarimeter quadrupole and boundary conditions are carefully included into the calculations.

We found the effect to be strongly dependent on positioning the detectors in a double–arm Möller polarimeter.

3 Dependence on the detector positions

The 'smearing' of the kinematics due to target electron motion changes asymmetry of the Möller scattering. This effect should be carefully calculated for any specific experimental set–up, since the magnitude of the effect depends on target thickness (via multiple scattering), polarimeter acceptances, magnetic optics, electron beam parameters, *etc.*

In our study, we have found a new effect due to Fermi–motion of atomic electrons. The effect is a dependence of the measured Möller asymmetry on the relative position of detectors in a double–arm mode. This effect can be understood from Figs. 1 and 2. Fig. 1 demonstrates the ratio of Möller asymmetry neglecting the effect of electron Fermi–motion to the same quantity but with the Fermi–motion included in the calculation, as a function of the detectors displacement from the symmetric around $\Theta^* = 90^0$ positions. Note that for the chosen electron energies and target thickness, the angular smearing due to Fermi–motion for K–electrons is an order of magnitude larger than due to multiple scattering in the target. Different displacements of the detectors in a double–arm mode result in a different effect due to Fermi motion on the Möller asymmetry. The correction is *positive* and reaches its maximum value for the case of symmetric position of the detectors, centered at the angle corresponding to 90^0–scattering angle in c.m.s.(denoted A in Fig. 2.) If the detectors are moved simultaneously toward larger (position B) or smaller (position C) angles, the Fermi–motion correction to the Möller asymmetry becomes *negative*. In absence of multiple scattering and the displacements lager than B or smaller than C (*e.g.*, position D), the Fermi–motion correction to the asymmetry would be exactly –100%. It means that we can observe a *zero* Möller asymmetry scattering polarized electron beam on atomic electrons with *nonzero* net polarization! The reason is that for this geometry of the experiment, we detect only the electrons scattered on unpolarized atomic shells. This polarization asymmetry of the detected electrons if $|\Delta\Theta_d/\Delta\Theta_{acc}| \geq 0.5$ is completly due to multiple scattering of electrons in the target. It may provide a direct measure of multiple scattering effect (*i.e.*, target thickness). Further displacing the detectors, the multiple scattering effect dies off exponentially, and the asymmetry of the electrons detected in coincidence approaches zero, but we may still observe a considerable amount of Möller electrons in coincidence coming from the tails of momentum distributions for atomic electrons.

The calculations in Fig. 1 were done for illustration, treating the polarimeter schematically as a target + a pair of detectors, with no magnets involved in the system. The acceptance (normalized to unity), the Fermi–motion smearing and multiple scattering angles were the same as for the realistic case described below.

Simulation of the Fermi–motion effect was done for the Möller polarimeter of CEBAF Hall A. A detailed description of this polarimeter is given in Ref. [8]. The polarimeter is designed for coincidence mode operation. The magnetic system includes two quadrupoles and a dipole. The simulation was done by RAYTRACE combined with a Monte–Carlo code for simulating Möller and multiple scattering. The results of the simulation are presented in Figs. 3, 4 for the electron beam energy $E_0 = 0.8$ GeV and target thickness $= 17.6\mu$m. The distribution of Möller electrons in the detector plane is demonstrated in Fig.3 for one of the detectors. For the other detector, the distribution is symmetric. The axis X is perpendicular to the reaction plane, and Y–axis indicates displacement with respect to the beam axis. The square area dashed with lines having a positive slope demonstrates the detector centered at Y_0 corresponding to $\Theta^* = 90^0$ ($\Theta_A = 35.7$ mrad). It provides the angular acceptance $\Delta\Theta/\Theta$=10.5%. The square dashed with lines having a negative slope demonstrates the detector displaced along the Y–axis by distance d. The second–arm

detector is displaced symmetrically with respect to the beam axis. The effect of this displacement is shown in Fig.4 and appears to be in qualitative agreement with the results of Fig.1 obtained for a simplified model of the polarimeter. As can be seen from Fig.4, the Fermi–motion effect is positive and maximal, reaching $\approx$10%, for small displacement d, wereas for large values of d, the effect is negative and may reach the magnitude of -100% completely eliminating the Möller asymmetry. The plot in Fig.4 is asymmetric with respect to d=0 due to dipole dispersion (it would become symmetric if plotted *vs.* angular shifts). The plateau (instead of a maximum like in Fig.1) is caused by additional boundary conditions set by the polarimeter magnetic system acting like an effective collimator.

It should be noted that the larger is the angular acceptance, the less Fermi motion affects the measured Möller asymmetry. We choose the beam energy E_0= 0.8 GeV for illustration because for higher energies, the angular acceptance of the polarimeter becomes large (25–42% for E_0=1.6–6.0 GeV) and the maximum positive Fermi–motion effect is small, not exceeding 3%.

4 Summary

We studied an effect of atomic electron Fermi–motion for a double–arm Möller polarimetry. We demonstrate that this effect may be either positive or negative depending on positioning of the detectors. If the detectors are centered at 90^0– scattering angle (in c.m.s.), the correction has a maximum positive value. For detectors shifted simultaneously toward larger/smaller angles, the effect becomes negative and may reach –100% completely eliminating the observed spin asymmetry. On the other hand, for a single–arm measurement the Fermi–motion correction remains positive despite the shift in the detector position.

Magnetic fields may essentially change electron kinematics, therefore, it is necessary to do detailed simulation of the polarimeter optical system in order to consistently calculate the electron Fermi–motion effect.

Acknowledgements

This work was supported by the US Department of Energy under contract DE–AC05–84ER40150.

A.A. would like to acknowledge useful discussions with his colleagues at CEBAF, Hampton University and KhPTI. A.G. would like to thank V.G. Gorbenko for collaboration in writing the Monte–Carlo simulation code for CEBAF Hall A Möller polarimeter.

References

[1] A.A. Kresnin and L.N. Rosentsveig, Journ. Exp. Theor. Phys. (USSR) 32, 1957, p.9353 (Soviet Physics JETP (1957) 288).

[2] L.Levchuk, The intra–atomic motion of bound electrons as a possible source of a systematic error in electron beam polarization measurements by means of a Möller polarimeter, Preprint KhPTI 92–32, Kharkov, 1992; Nucl. Instr. and Meth. A311 (1994) 496.

[3] M. Swartz, H.R. Band, F.J. Decker et al., Nucl. Instr. and Meth. A363 (1995) 526.

[4] A. Afanasev, Parallel talk at Spin '94, Bloomington, IN, September 1994, unpublished.

[5] AIP Handbook, (1993).

[6] J. Arrington, E.J. Beise, B.W. Fillipone et al., Nucl. Instr. and Meth. A311 (1992) 39, and B. Fillipone, private communication.

[7] K.B.Beard, R. Madey, W.M. Zhang et al., Nucl. Instr. and Meth. A361 (1995) 46.

[8] Möller polarimeter for Hall A, A.Glamazdin, V.Gorbenko et al., CEBAF, January 1996.

Figure Captions

Figure 1. Fermi–motion correction to the Möller asymmetry for ^{26}Fe target as a function of detectors displacement, $\Delta\Theta_d$ being the displacement angle with respect to $\Theta^*= 90^0$, $\Delta\Theta_{acc}$ being the angular acceptance, and $A(A_0)$ being the asymmetry with (without) the Fermi–motion correction.

Figure 2. Schematic positions of the detectors. The angle Θ_A corresponds to $\Theta^*= 90^0$, and the positions A, B, C, and D correspond to $\Delta\Theta_d/\Delta\Theta_{acc}$= 0, 0.5,-0.5, >0.5, respectively, in Fig.1.

Figure 3. Simulated distribution of Möller events in the detector plane of CEBAF Hall A Möller polarimeter. Dashed square areas show different positions of the detectors. The notations are explained in the text.

Figure 4. Simulated Fermi–motion effect for CEBAF Hall A Möller polarimeter as a function of the detectors displacement d, as shown in Fig.3.

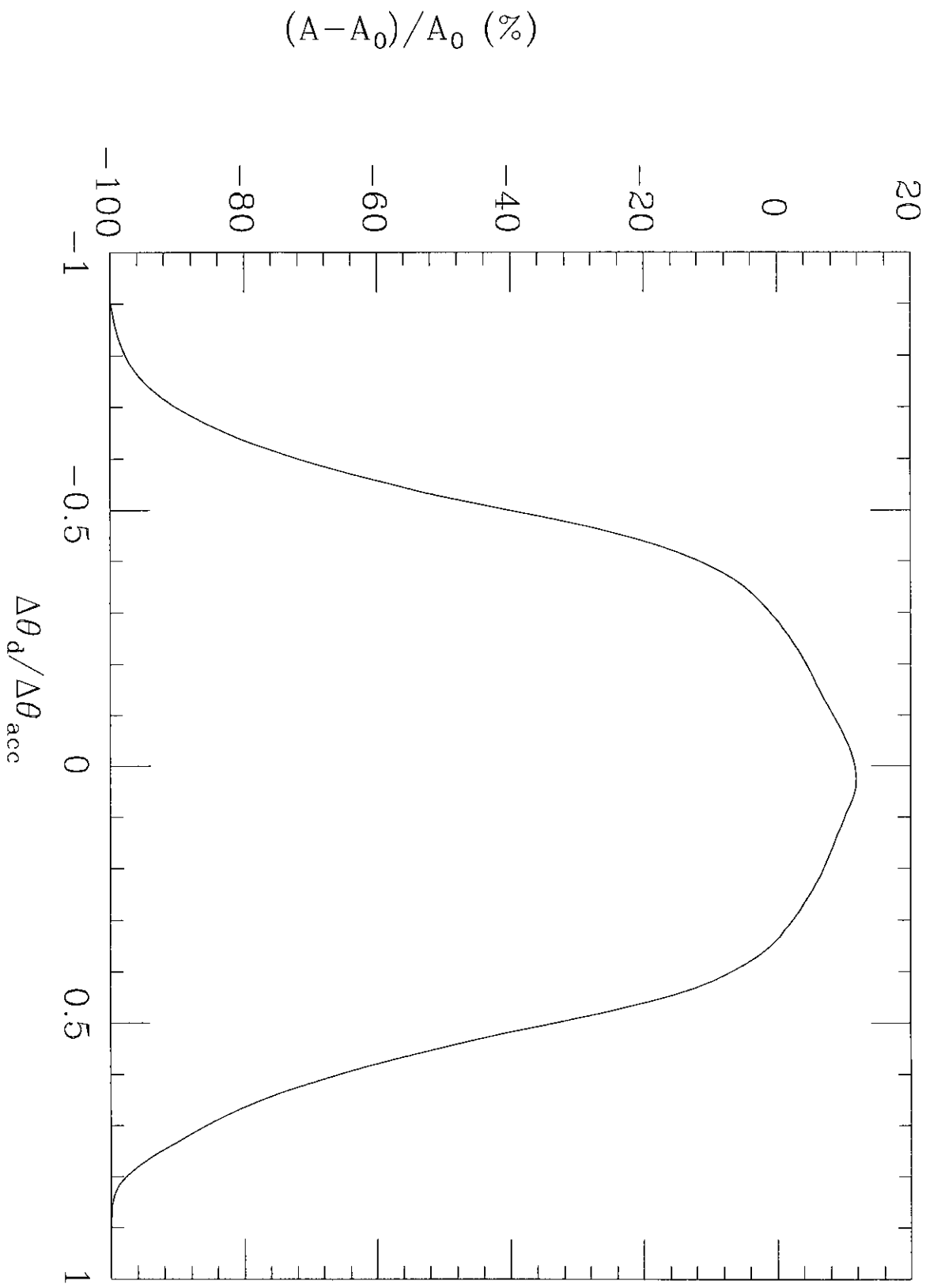
20
0
−20
−40
−60
−80
−100
−1
−0.5
0
0.5
1
$\Delta\theta_d/\Delta\theta_{acc}$
$(A-A_0)/A_0$ (%)

Figure 1

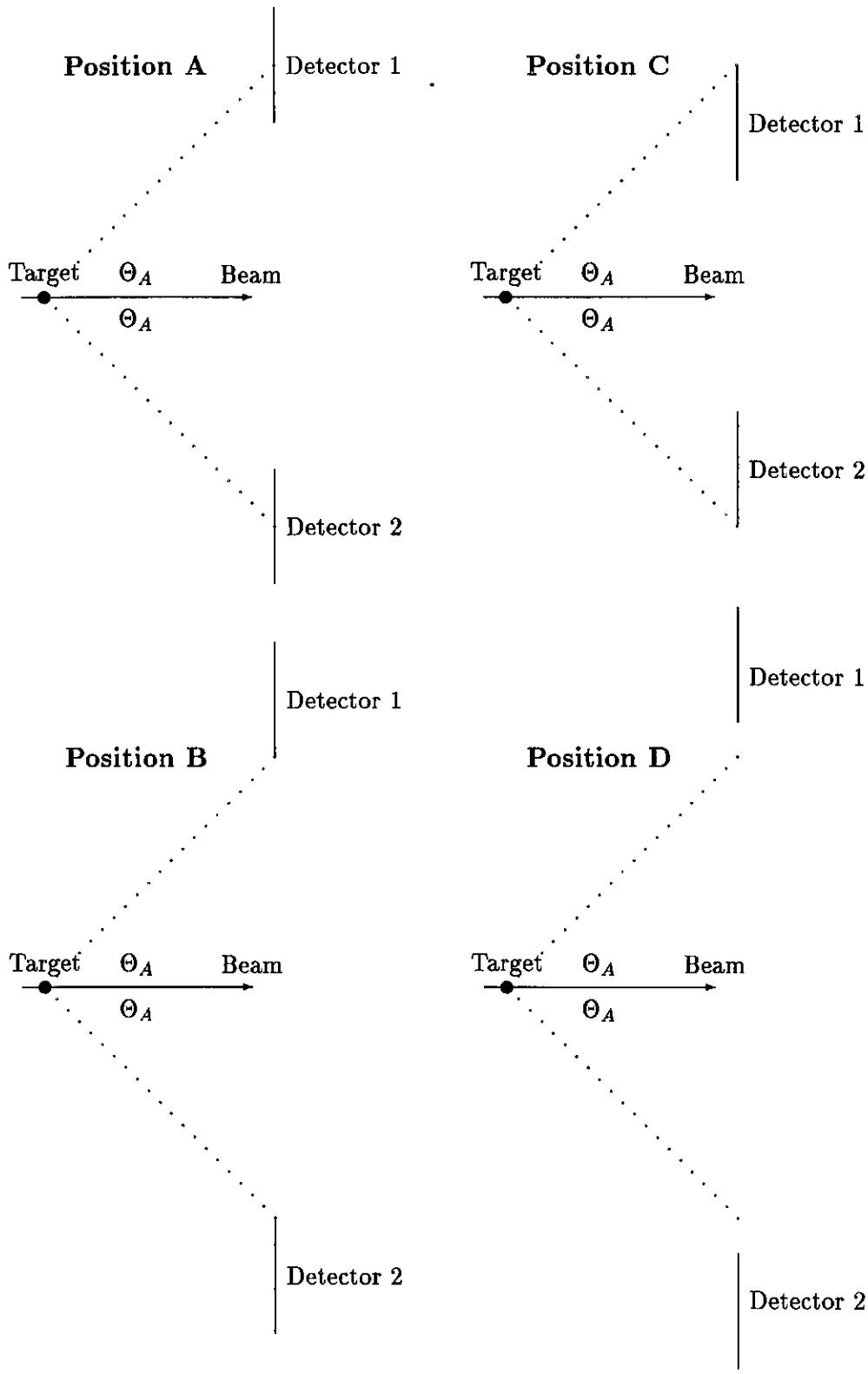
Position A
Detector 1
Target
Θ_A
Beam
Θ_A
Detector 2
Position C
Detector 1
Target
Θ_A
Beam
Θ_A
Detector 2
Detector 1
Position B
Target
Θ_A
Beam
Θ_A
Detector 2
Detector 1
Position D
Target
Θ_A
Beam
Θ_A
Detector 2

Figure 2

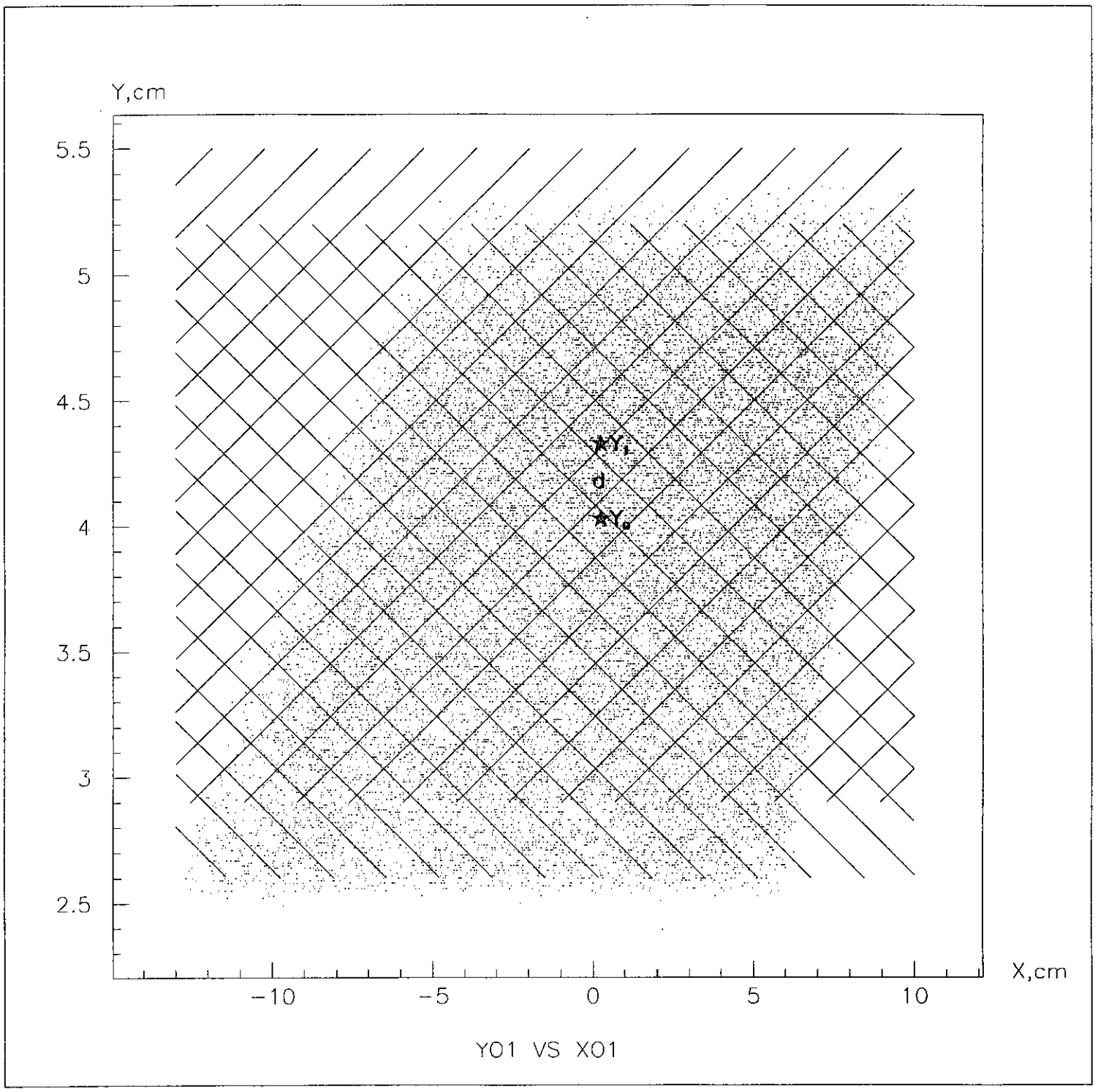

Figure 3

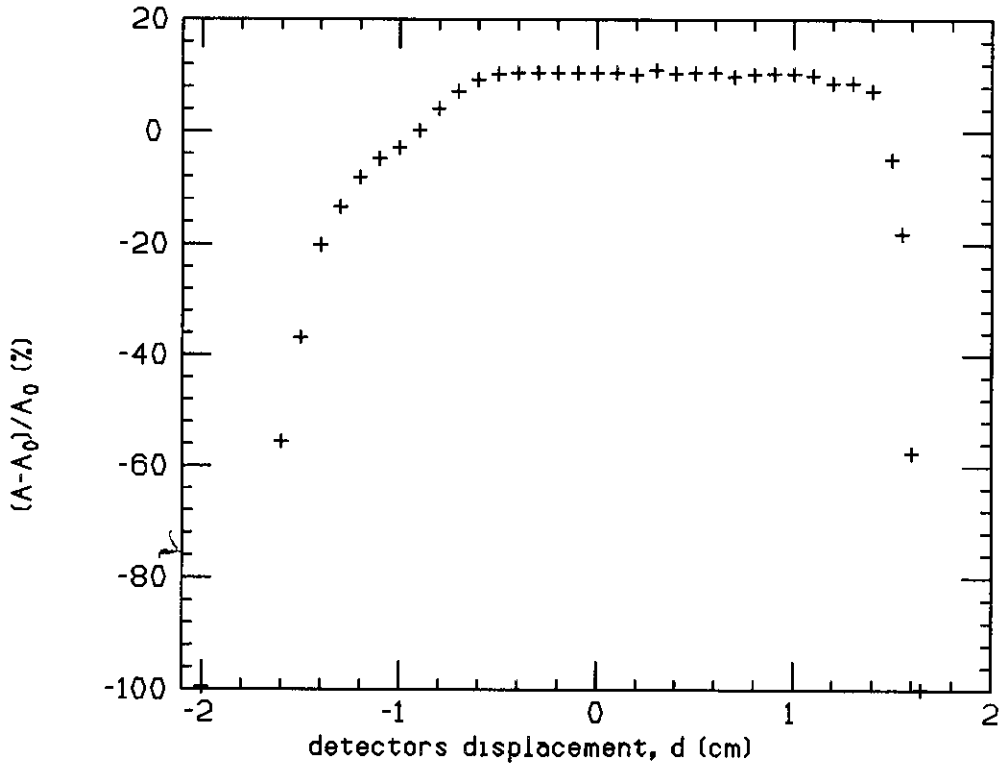

Figure 4